Inorganic Chemistry Research

Article

# Synthesis, Spectral Characterization, and Theoretical Investigation of Pd(II) Complex Incorporating Unsymmetrical Tetradentate Schiff Base Ligand and its Application in Suzuki-Miyaura Cross-Coupling Reaction

Hadi Kargar[a,*], Mehdi Fallah-Mehrjardi[b], Reza Behjatmanesh-Ardakani[b], Khurram Shahzad Munawar[c,d], Mehrnaz Bahadori[e] and Majid Moghadam[e]

[a]*Department of Chemical Engineering, Faculty of Engineering, Ardakan University, P.O. Box 184, Ardakan, Iran*
[b]*Department of Chemistry, Payame Noor University (PNU), 19395-4697, Tehran, Iran*
[c]*Department of Chemistry, University of Sargodha, Punjab, Pakistan*
[d]*Department of Chemistry, University of Mianwali, Mianwali, Pakistan*
[e]*Catalysis Division, Department of Chemistry, University of Isfahan, 81746-73441, Isfahan, Iran*

Received: April 15, 2022; Accepted: May 31, 2022
**Cite This:** *Inorg. Chem. Res.* **2022**, *6*, 76-83. DOI: 10.22036/icr.2022.337714.1128

**Abstract:** A new palladium(II) complex is synthesized *via* the treatment of unsymmetrical tetradentate Schiff base ($\mathbf{H_2L^{Uns}}$) with $Pd(CH_3COO)_2$. An analytical technique like combustion analysis for the estimation of C, H, and N and other spectroscopic techniques such as FT-IR and $^1H$ NMR were used to elucidate the structural confirmation of the synthesized complex. Furthermore, the theoretical parameters of the optimized structures calculated by the DFT employing the B3LYP/Def2-TZVP level of theory were carried out to correlate the calculated findings with the actual data obtained experimentally. The spectroscopic and theoretical data findings revealed that the ligand is coordinated *via* phenolic oxygen and imine nitrogen atoms. Moreover, the catalytic activity of the palladium(II) complex was studied in the Suzuki-Miyaura cross-coupling reactions (SMCR).

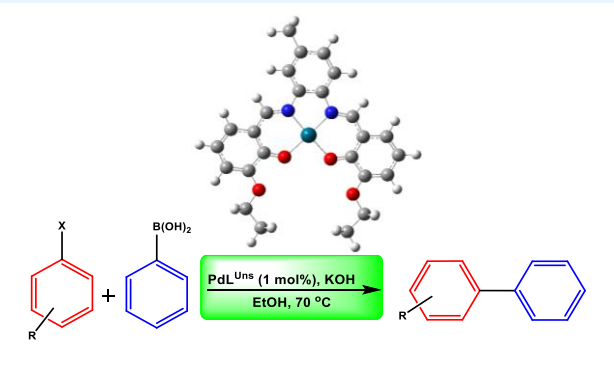


**Keywords:** Schiff base, Palladium(II), Theoretical investigation, Suzuki-Miyaura reaction

## 1. INTRODUCTION

Schiff bases belong to a multinucleated class of ligands with various kinds of donor atoms that form complexes with almost all kinds of metal atoms.[1-3] The significant features such as facile accessibility, relatively inexpensive, specificity and sensitivities, and chelation to core metal ions, have led to a surge in interest in these moieties over the last decade.[4-8] In coordination chemistry, tetradentate Schiff base is among the most investigated ligands. They can coordinate with a wide number of transition metals and have a variety of intriguing catalytic and electrochemical properties.[9] The ONNO tetradentate donor set is one form of tetradentate Schiff base ligand that has a number of advantages, including ease of use, relative tolerability, easily modified auxiliary ligands, and tunability of steric and electronic coordination environments on the metal centre.[10,11]

Salophen is a very familiar class of diamine tetradentate ligands, generally, with an ONNO core that chelates with a metal ion in its deprotonated form[12] to produce neutral metal complexes on coordination with metal ions in their divalent form.[13] Salophen ligands, a generic term for Schiff bases derived *via* condensation of salicylaldehyde and *o*-phenylenediamine derivatives, provide a tetradentate (ONNO) chelating system that allows for the production of stable metal complexes with significant $\pi \rightarrow \pi^*$ intramolecular electronic interactions.[14]

For a wide range of chemical reactions like hydrosilylation, homogeneous catalysis, transfer hydrogenation, C-C coupling reactions, and epoxidation, Schiff base complexes show strong catalytic activity.[15] Researchers are attempting to develop simple, rapid, cheap, and efficient approaches.[16] The Suzuki-Miyaura reaction, one of the most prominent C-C cross-coupling

reactions today, is the utmost significant reaction between aryl halides and arylboronic acids and is commonly utilized to create biaryls. Biaryls are a widely used component in a variety of industrial applications, including medicines, natural products, agrochemicals, advanced materials, and cosmetics.[17,18] For coupling reactions, like Heck and Suzuki,[19,20] palladium complexes comprising salophen based ligands have been thoroughly studied and the geometry of metal salophen complexes tends to be square-planer.[21]

The effectiveness of catalytic systems comprising either $Pd^0$ or $Pd^{+2}$ derivatives connected with suitable ligands can be enhanced by changing the environment surrounding the Pd center.[22-24] When aryl bromides or iodides are used as precursors, the products are generated with a higher yield than when aryl chlorides are used. It's worth noting that in SMCR using palladium catalysts, aryl halides are generally activated in the following order: R-I > R-Br > R-Cl.[25]

The structural and electrical characteristics of the metal complexes containing Schiff base ligands can be studied using density functional theory. In the literature, DFT and TD-DFT approaches were used to optimize the geometry, structures, and theoretical parameters of various salophen-based metal complexes.[12]

In light of the aforementioned applications and based on our previous findings of the Schiff bases and their transition metal complexes,[26-37] the goal of this study is to prepare a Pd-based salophen type complex for its potential application as a catalyst in SMCR.

## 2. EXPERIMENTAL

### Materials and methods

All of the precursors employed in the present work are laboratory quality and were obtained from Daejung, Alfa Aesar, and Panreac. The Heraeus CHN-O-FLASH EA 1112 equipment was employed to determine the chemical constituents of the synthesized compounds. Using BRUKER AVANCE 400 MHz spectrometers, the 1H NMR spectral data was collected. The signals were allocated chemical shift (δ) values in ppm after comparing them with the value exhibited by tetramethylsilane (TMS). Furthermore, the vibrational details of different functional groups associated with the molecules under investigation were calculated by the IRPrestige-21 spectrophotometer through the KBr pellet method.

### Synthesis

**Synthesis of unsymmetrical salophen based tetradentate Schiff base ligand ($H_2L^{Uns}$).** To a 150 mL round bottom flask, 4-methyl-1,2-phenylenediamine (1 mmol) was mixed with an ethanolic solution (50 mL) of 3-ethoxysalicylaldehyde (2 mmol, 0.332 g) with continuous stirring. Subsequently, the precursors were refluxed for approximately one hour until the orange solid product **($H_2L^{Uns}$)** was produced. The purity of the produced sample was further supported by TLC. The **$H_2L^{Uns}$** was separated by filtration, washed in triplicate with ethanol, and finally dried in a desiccator in a dehydrating environment.

**$H_2L^{Uns}$.** (6,6'-((1E,1'E)-((4-methyl-1,2-phenylene)bis(azanylylidene))bis(methanylylidene))bis(2-ethoxyphenol)):
Yield 89%. Anal. Calc. for $C_{25}H_{26}N_2O_4$: C, 71.75; H, 6.26; N, 6.69, Found: C, 71.87; H, 6.30; N, 6.58 %. FT-IR (KBr, $cm^{-1}$); 1616 ($\upsilon_{C=N}$); 1558, 1474 ($\upsilon_{C=C}$); 1277 ($\upsilon_{C-O}$). $^1$H NMR (400 MHz, $CDCl_3$, ppm): 1.15 [3H, t, (-$CH_3$), $^3J$ = 7.2 Hz], 1.25 [3H, t, (-$CH_3$), $^3J$ = 7.2 Hz], 2.36 [3H, s, (-$CH_3$)], 4.06 [2H, q, (-$CH_2$-O), $^3J$ = 7.2 Hz], 4.13 [2H, q, (-$CH_2$-O), $^3J$ = 7.2 Hz], 7.40-7.78 [9H, m, aromatic], 8.97 [1H, s, (-CH=N)], 8.98 [1H, s, (-CH=N)], 12.95 [1H, s, (-OH)], 13.02 [1H, s, (-OH)].

**Synthesis of palladium(II) complex ($PdL^{Uns}$).** To make the palladium(II) complex, the equimolar amount of synthesized Schiff base **($H_2L^{Uns}$)** was mixed with a 25 mL hot methanolic solution of $Pd(CH_3COO)_2$. The reagents were refluxed while being constantly stirred for around 3 h. The transparent red solution thus formed was kept as such for crystallization after being covered partly with a layer of aluminium foil for gradual evaporation. After 4-5 days, deep-red crystals of **$PdL^{Uns}$** were formed.

**$PdL^{Uns}$.** Yield 61%. Anal. Calc. for $C_{25}H_{24}N_2O_4Pd$: C, 57.43; H, 5.36; N, 5.90, Found: C, 57.54; H, 5.38; N, 5.82 %. FT-IR (KBr, $cm^{-1}$); 1589 ($\upsilon_{C=N}$); 1539, 1431 ($\upsilon_{C=C}$); 1330 ($\upsilon_{C-O}$); 590 ($\upsilon_{Pd-O}$); 497 ($\upsilon_{Pd-N}$). $^1$H NMR (400 MHz, DMSO-$d_6$, ppm): 0.86 [3H, t, (-$CH_3$), $^3J$ = 7.2 Hz], 0.97 [3H, t, (-$CH_3$), $^3J$ = 6.8 Hz], 2.17 [3H, s, (-$CH_3$)], 3.88 [2H, q, (-$CH_2$-O), $^3J$ = 7.2 Hz], 3.94 [2H, q, (-$CH_2$-O), $^3J$ = 6.8 Hz], 6.96-7.53 [9H, m, aromatic], 9.35 [1H, s, (-CH=N)], 9.36 [1H, s, (-CH=N)].

### Computational details

All DFT parameters were calculated using the Gaussian code,[38] the B3LYP hybrid approach,[39] and the Def2-TZVP basis set.[40] The solution phase was modelled using the IEFPCM method, which incorporated interactions between the solute and the solvent.[41] After optimization, a frequency analysis was conducted to check that the proposed structures were at the local minimum of the molecular potential energy surface. All imaginary frequencies were zero in all frequency analysis studies, indicating that all designed molecules are at local minimum points.

The nuclear magnetic resonance (NMR) data were determined using Gauge-Independent Atomic Orbital (GIAO) approach.[42] Chemical shifts (δ) of the **$H_2L^{Uns}$** ligand and **$PdL^{Uns}$** complex in deuterated solvents ($CDCl_3$/DMSO-$d_6$) were done at B3LYP/Def2-TZVP. The chemical shift (δ) values were assigned by subtracting the corresponding isotropic component of the shielding tensor from tetramethylsilane. The B3LYP/Def2-TZVP level of theory was used to estimate the solution phase isotropic shielding constants for tetramethylsilane, which were found to be 31.92 ppm for the $^1$H nuclei. The Chemissian software[43] was utilized to construct contour plots of the lowest unoccupied molecular orbital (LUMO) and the highest occupied molecular orbital (HOMO). The molecular electrostatic potential (MEP) was also determined with the help of Gaussian and GaussView programmes. Data related to natural bond orbitals (NBO) was also collected using the NBO 6.0 software.[44]

### General procedure for Suzuki-Miyaura cross-coupling reaction catalyzed by $PdL^{Uns}$

**$PdL^{Uns}$** (5 mg including 0.01 mmol Pd(II)) was added to a mixture of aryl halide (1 mmol), phenylboronic acid (2 mmol),

KOH (2.4 mmol), and EtOH (3 mL) in a three-necked round-bottom. The mixture was stirred at desired time and temperature under inert gas. Gas chromatography was used to track the reaction's progression.

## 3. RESULTS AND DISCUSSION

### Synthesis

The treatment of 4-methyl-1,2-phenylenediamine with 3-ethoxysalicylaldehyde in ethanol produced the salophen-based unsymmetric tetradentate ONNO Schiff base ligand (**$H_2L^{Uns}$**). The **$PdL^{Uns}$** complex is formed by reacting palladium acetate with **$H_2L^{Uns}$** in refluxing methanol, as shown in Scheme 1.

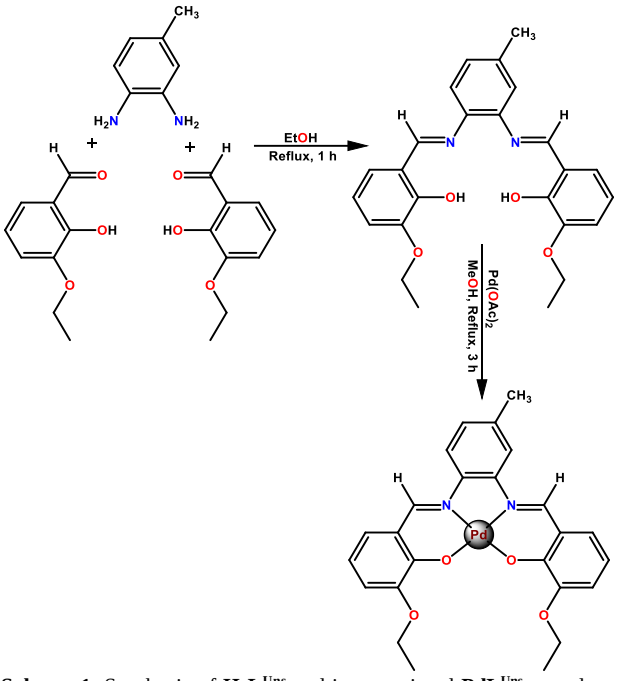


**Scheme 1.** Synthesis of **$H_2L^{Uns}$** and its associated **$PdL^{Uns}$** complex

### FT-IR spectra

The key stretching vibrational bands/peaks of the synthesized ligand and its associated palladium complex are shown in Figure S1. The chief coordinating points of the ligand that are going to participate in complexation were sorted out by co-relating the FT-IR spectrum of ligand with that of complex. At 1616 $cm^{-1}$, an interesting peak for the HC=N moiety was detected, which was shifted to a lower wavenumber (1589 $cm^{-1}$) in the palladium complex.[45] This is because the chelation of nitrogen atoms to the metal centre resulted in a reduction in the electronic density, which is compatible with the previous findings from structurally related molecules.[46] On chelation, the locations of stretching vibrational bands belonging to C–O in the unchelated ligand (1277 $cm^{-1}$) are changed to a higher frequency area (1330 $cm^{-1}$) because of the engagement of oxygen atoms in complexation.[47] Finally, the chelation of azomethine nitrogen and phenolic oxygen atoms with the metal center is further revealed by the appearance of weak bands at low wavenumbers that were caused by the presence of metal-N and metal-O linkages.[48]

The gaseous phase IR stacked spectrum of the produced compounds proposed by the B3LYP/Def2-TZVP level of theory is illustrated in Figure S2. The higher level of the resemblance between the actual and theoretically calculated spectral data is an indication of the close association of the molecular structures of the produced compounds in solid and gaseous states. Table S1 summarizes the compounds' experimental and theoretically calculated vibrational frequencies, as well as relative errors (%). The computed vibrational frequencies were multiplied with a scaling factor of 0.965[49] to attain the rectified results that were consistent with actual findings. Due to the employment of harmonic estimation for computations performed in a vacuum, the highest notable variation between these two groups of findings is only 0.56 percent.

### $^1$H NMR spectral details

$^1$H NMR spectrum of the **$H_2L^{Uns}$** was taken using $CDCl_3$ as a deuterated solvent, while the magnetic data of the corresponding palladium complex was measured in DMSO-$d_6$. In addition, the experimental section specifies the $^1$H NMR spectral features of the synthesized compounds, and the spectra are displayed in Figures S3 & S4. The phenolic protons of **$H_2L^{Uns}$** are ascribed to the major peak in the $^1$H NMR spectrum at $\delta$ = 12.95 and 13.02 ppm. This suggests that the phenolic oxygens are effectively linked to the metal upon discharging their protons. The relocation of signals for HC=N in the $^1$H NMR spectrum of the investigated complex is compatible with FT-IR results showing that the signals for the azomethine linkage in the spectrum of the complex are visible at a lower wavenumber value than for an uncomplexed substrate. The aromatic protons in the magnetic spectrum of **$H_2L^{Uns}$** are detected in anticipated locations between 7.40 and 7.78 ppm. The position of peaks for aromatic protons varies inconsequentially during chelation ($\delta$ = 6.96-7.53 ppm), while peaks of the aliphatic protons fail to express a noteworthy shift in their location after chelation. Table S2 summarises the experimental and computational findings related to the $^1$H NMR of the **$H_2L^{Uns}$** and its corresponding **$PdL^{Uns}$**, indicating that the data are in excellent accordance.

### Structural optimization

The molecular structures of the synthesized compounds were optimized to find the local minimum using the B3LYP/Def2-TZVP approach to evaluate their respective geometrical parameters. Figure 1 illustrates the gas phase structural optimization of the synthesized compounds.

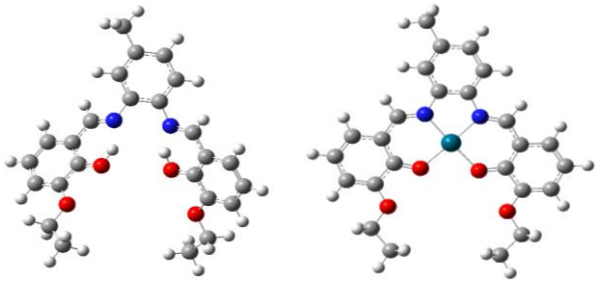

$H_2L^{Uns}$ $PdL^{Uns}$

**Figure 1.** Optimized geometrical illustration of unsymmetrical ligand and its corresponding Pd complex.

### Frontier molecular orbitals investigation

In quantum chemistry calculations, the energy gap (ΔE) of the frontier molecular orbitals (FMOs) is a perilous feature. FMO analysis demonstrates the kinetic stability and chemical activity of the compounds under investigation. Chemical hardness is a valuable indicator for assessing the chemical stability of molecules.[50] Species having a small ΔE value are referred to as "soft," whereas the moieties having a higher ΔE value are referred to as "hard." Softer compounds appear to be easily polarizable in the view of the fact that overcoming the difference in energy ($\Delta E = E_{LUMO} - E_{HOMO}$) requires less energy.[51] The B3LYP technique was used to calculate the electronic parameters of the synthesized compounds using a Def2-TZVP basis set. Figure 2 depicts the HOMO and LUMO of the compounds, while Table 1 lists their quantum chemical characteristics.

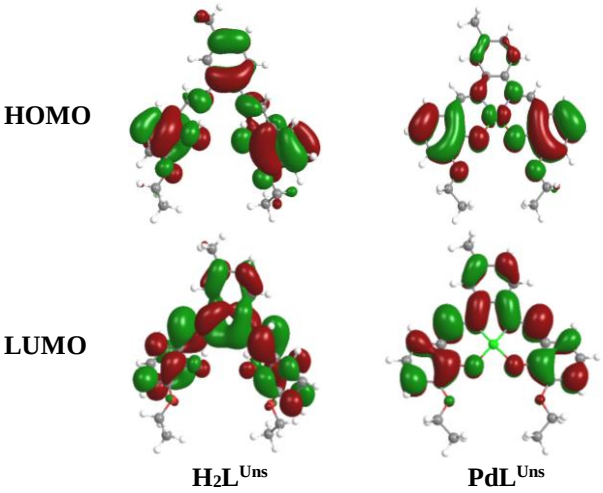


**Figure 2.** FMOs of the $H_2L^{Uns}$ and its $PdL^{Uns}$.

lower as compared to $H_2L^{Uns}$, which makes it a softer compound. The compounds' hardness and softness data give similar results. As a result, the $PdL^{Uns}$ is more reactive as compared to the ligand. The negative values of chemical potential confirm the stability of the synthesized compounds. In addition to this, the higher electrophilicity index value for $PdL^{Uns}$ demonstrates its strong electrophilic nature as compared to $H_2L^{Uns}$.

### Molecular electrostatic potential (MEP) maps

The MEP is a useful and chief metric for defining the nucleophilic and electrophilic behaviour of species under investigation. The electrostatic area is highlighted in the MEP analysis in addition to the molecular size and shape. It is a useful technique to investigate structural connections and photochemical characteristics of the investigated molecules with respect to color scaling. The red, blue, and green colors in MEP denote the negative, positive, and neutral electrostatic sections.[52] MEPs were calculated using B3LYP/Def2-TZVP to investigate the ligand and complex's nucleophilic and electrophilic interacting sites, as shown in Figure 3. The more electronegative atoms in the ligand, such as O and N atoms, have the most negative regions, while protons have the most positive areas. The blue colour of the complex depicts that the Pd atom, which is present near the centre of the positive electrostatic area, is an exceptional site for a nucleophilic interaction. The majority of negative charges are found in the vicinity of O and N atoms, which are the primary protons' targets.

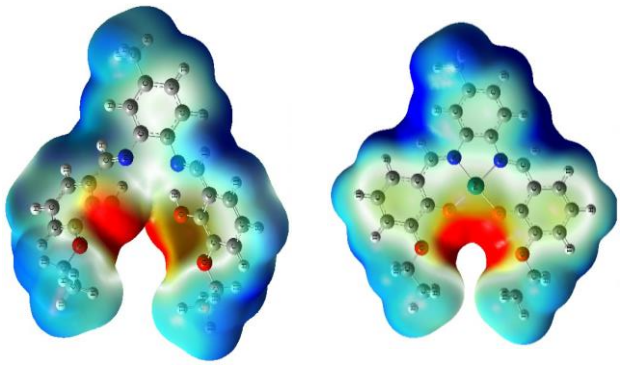

$H_2L^{Uns}$ $PdL^{Uns}$

**Figure 3.** MEP maps of the $H_2L^{Uns}$ and $PdL^{Uns}$.

### Natural bond orbital (NBO) analysis

The natural bond orbital (NBO) study utilizes second-order perturbations to calculate the stabilization energy of

**Table 1.** Quantum chemical descriptions of $H_2L^{Uns}$ and $PdL^{Uns}$ (in eV)[a]

| | $E_{HOMO}$ | $E_{LUMO}$ | ΔE | I | A | η | S | χ | μ | ω |
|---|---|---|---|---|---|---|---|---|---|---|
| $H_2L^{Uns}$ | -5.928 | -2.176 | 3.752 | 5.928 | 2.176 | 1.876 | 0.267 | 4.052 | -4.052 | 4.376 |
| $PdL^{Uns}$ | -5.481 | -2.452 | 3.029 | 5.481 | 2.452 | 1.514 | 0.330 | 3.966 | -3.966 | 5.195 |

[a]ΔE = Energy gap ($E_{LUMO} - E_{HOMO}$); I = Ionization potential ($-E_{HOMO}$); A = Electron affinity ($-E_{LUMO}$); η = Hardness ((I - A)/2); S = Softness (1/2η); χ = Electronegativity ((I + A)/2); μ = Chemical potential (-(I + A)/2); ω = Electrophilicity ($\mu^2/2\eta$).

the interactions between donor and acceptor species. The NBO is indeed a fine place to begin if you want to learn more about charge transfer in molecular species.[53]
Using the B3LYP/Def2-TZVP technique, the complexes' NBO analysis revealed the foremost electron donor and acceptor orbitals. The furthermost significant relations are between nonbonding lone pairs of O and N atoms as donors, while vacant d-orbitals of $Pd^{+2}$ as acceptors. Figure 4 depicts the interactions of donor-acceptor orbitals in the **PdL$^{Uns}$** complex from LP (2) $O_1$, LP (2) $O_3$, LP (1) $N_1$, and LP (1) $N_2$ to LV (1) $Pd_1$.

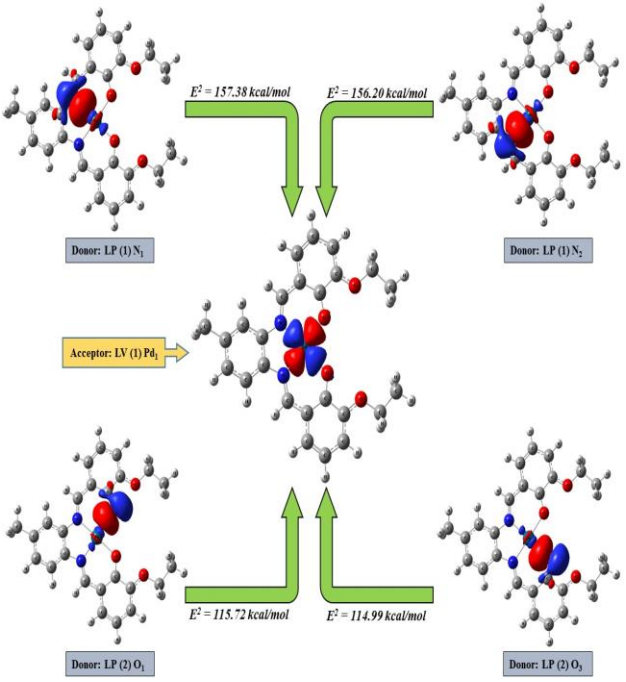


**Figure 4.** Donation of electrons from LP (2) $O_1$, LP (2) $O_3$, LP (1) $N_1$ and LP (1) $N_2$ to LV (1) $Pd_1$ in **PdL$^{Uns}$**.

The catalytic performance of the **PdL$^{Uns}$** was examined in light of palladium's efficiency in the SMCR. The chemical reaction between phenylboronic acid and 4-iodoanisol was selected as the standard reaction, and the reaction parameters, including, base, solvent, temperature, and catalyst quantity, were altered to determine optimal parameters for the maximum yield. Table 2 shows a summary of the findings. Several solvents or their mixtures with $H_2O$ were examined (Table 2, Entries 1-5), and the standard reaction provided the maximum yield for using ethanol (Table 2, Entry 5).
Various quantities of **PdL$^{Uns}$** were selected to achieve the least active quantity in the standard reaction, demonstrating the importance of pricing in catalytic systems (Table 2, Entries 5-7). The superlative TOF was attained when a 5 mg **PdL$^{Uns}$** (1 mol%) was used, and this amount was used in the next phases (Table 2, Entry 5). Although the yield of the product fell at 60 °C, the catalytic performance of **PdL$^{Uns}$** did not demonstrate a significant improvement in yield at 78 °C as listed in Table 2, with entries 8 and 9. The optimum temperature with an appropriate yield was then determined to be 70 °C.
The base also plays an important role in the SMCR as it activates boronic acid. Several types of bases were investigated in the catalysis scheme employing the **PdL$^{Uns}$** to discover the most capable and versatile one (Table 2, Entries 10-17). The maximum yield was produced in the presence of KOH, according to the findings (Table 2, Entry 12). The best yield was obtained using 1 mol% **PdL$^{Uns}$** complex to react 2 mmol phenylboronic acid and 1 mmol 4-iodoanisol in 3 mL ethanol at 70 °C in 2.4 mmol KOH.
The **PdL$^{Uns}$** complex was used to study the reaction between the scope of aryl halide and phenylboronic acid to determine its performance under optimal conditions.

**Table 2.** Optimization of the reaction conditions in SMCR using **PdL$^{Uns}$**, [a]

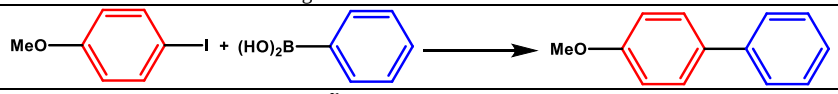


| Entries | Solvent | PdL$^{Uns}$ (mol%) | T (°C) | Base | Time (h) | Yield (%)[b] |
|---|---|---|---|---|---|---|
| 1 | DMF/$H_2O$ (2/1) | 1 | 70 | $K_2CO_3$ | 12 | 71 |
| 2 | Ethanol/$H_2O$ (2/1) | 1 | 70 | $K_2CO_3$ | 12 | 65 |
| 3 | $CH_3CN$/$H_2O$ (2/1) | 1 | 70 | $K_2CO_3$ | 12 | 47 |
| 4 | DMF | 1 | 70 | $K_2CO_3$ | 24 | 29 |
| 5 | Ethanol | 1 | 70 | $K_2CO_3$ | 6 | 94 (15.7)[c] |
| 6 | Ethanol | 0.5 | 70 | $K_2CO_3$ | 10 | 72 (14.4)[c] |
| 7 | Ethanol | 1.5 | 70 | $K_2CO_3$ | 5 | 95 (12.7)[c] |
| 8 | Ethanol | 1 | 78 | $K_2CO_3$ | 5 | 94 |
| 9 | Ethanol | 1 | 60 | $K_2CO_3$ | 10 | 78 |
| 10 | Ethanol | 1 | 70 | KOAc | 10 | 18 |
| 11 | Ethanol | 1 | 70 | $K_2HPO_4$ | 10 | 29 |
| 12 | Ethanol | 1 | 70 | KOH | 5 | 94 |
| 13 | Ethanol | 1 | 70 | $Na_2CO_3$ | 10 | 31 |
| 14 | Ethanol | 1 | 70 | $NaH_2PO_4$ | 10 | 37 |
| 15 | Ethanol | 1 | 70 | $Na_2HPO_4$ | 10 | 30 |
| 16 | Ethanol | 1 | 70 | $Na_3PO_4$ | 10 | 63 |
| 17 | Ethanol | 1 | 70 | $NEt_3$ | 10 | 24 |

[a]Reaction conditions: Phenylboronic acid (2 mmol), 4-iodoanisol (1 mmol), solvent (3 mL), base (2.4 mmol). [b]Determined by GC. [c]TOF ($h^{-1}$).

The results of using aromatic chloride, aromatic bromide, and aromatic iodide with various substituents as functional groups may be found in Table 3. Except for the aryl chloride, which had a modest yield due to the stronger C to Cl bond, remarkable yields were achieved utilizing other aromatic halides, confirming **PdL$^{Uns}$** complex's superb performance in SMCR.

**Table 3.** SMCR for various aryl halides using **PdL$^{Uns}$**, [a]

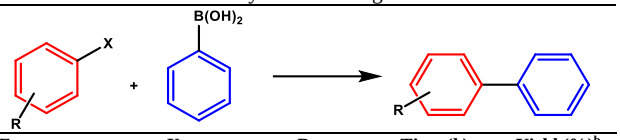


| Entry | X | R | Time (h) | Yield (%)[b] |
|---|---|---|---|---|
| 1 | I | H | 4 | >99 |
| 2 | I | 4-$OCH_3$ | 5 | 94 |
| 3 | I | 4-$CH_3$ | 5.5 | 91 |
| 4 | Br | H | 5.5 | 97 |
| 5 | Br | 4-$COCH_3$ | 8 | 82 |
| 6 | Br | 3-CN | 8 | 84 |
| 7 | Cl | H | 9.5 | 95 |
| 8 | Cl | 4-$NO_2$ | 11 | 47 |
| 9 | Cl | 2-$NO_2$ | 8 | 53 |
| 10 | Cl | 3-$COCH_3$ | 24 | 74 |
| 11 | Cl | 4-CN | 24 | 59 |

[a]Reaction conditions: aromatic halide (1 mmol), KOH (2.4 mmol), phenylboronic acid (2 mmol), EtOH (3 mL), **PdL$^{Uns}$** (1 mol%) at 70 °C. [b]Determined by GC.

Scheme 2 represents the proposed mechanism for the Suzuki-Miyaura coupling reaction using **PdL$^{Uns}$**. First, Pd(II) produces Pd(0) during the reduction reaction and it follows by ox-add. Aryl halide adds to the Pd complex and **B** containing Pd(II) is generated. The base replaces halide with OH in **B** structure and aryl group in phenylboronic acid, in the presence of a base, produces **D**. The cycle would be completed with giving biphenyl and the Pd(0) regenerates again.

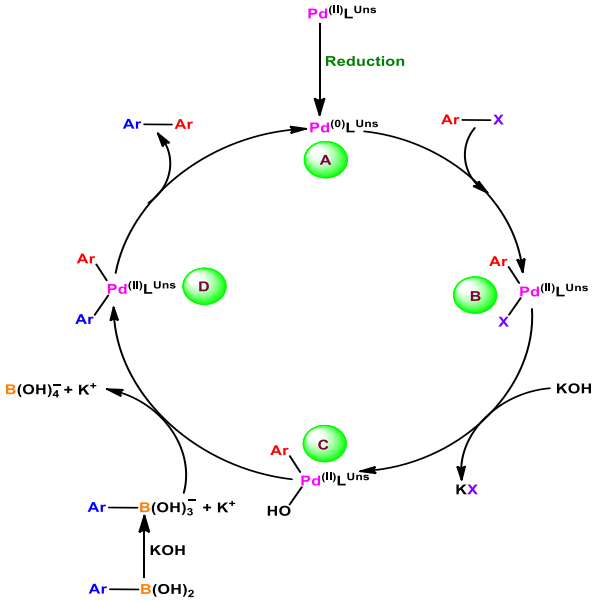


**Scheme 2.** The purposed mechanism for Suzuki-Miyaura C-C coupling using **PdL$^{Uns}$**

## 5.CONCLUSIONS

The present work illustrates that an unsymmetrical Schiff base ligand (**$H_2L^{Uns}$**) and its **PdL$^{Uns}$** complex are successfully prepared, structurally investigated, and theoretically correlated with the actual structures. The FT-IR and $^1$H NMR data confirm the points of chelation and tetradentate nature of the ligand. The DFT studies show that the **PdL$^{Uns}$** complex has a smaller ΔE value than the synthesized ligand, making it softer and more reactive moiety. The MEP analysis sorted out that oxygen and nitrogen atoms are the most negative areas in the ligand, Protons, on the other hand, have the most positive regions. Furthermore, outstanding yields were attained employing different aromatic halides, demonstrating the **PdL$^{Uns}$** complex's exceptional catalytic activity in SMCR.

## CONFLICTS OF INTEREST

The authors declare that they have no known competing financial interests or personal relationships that could have appeared to influence the work reported in this paper.

## ACKNOWLEDGEMENTS

We gratefully acknowledge the practical support of this study by Ardakan University and Payame Noor University.

## AUTHOR INFORMATION

**Corresponding Author**

Hadi Kargar: Emails: h.kargar@ardakan.ac.ir; hadi_kargar@yahoo.com, *ORCID*: 0000-0002-7817-0937

**Author(s)**

Mehdi Fallah-Mehrjardi, Reza Behjatmanesh-Ardakani, Khurram Shahzad Munawar, Mehrnaz Bahadori, Majid Moghadam

## REFERENCES

1. S. Shit, M. Nandy, D. Saha, L. Zhang, W. Schmitt, C. Rizzoli, T. N. G. Row, *J. Coord. Chem.* **2016**, *69*, 2403-2414.
2. Z. Beigi, A. H. Kianfar, H. Farrokhpour, M. Roushani, M. H. Azarian, W. A. K. Mahmood, *J. Mol. Liq.* **2018**, *249*, 117-125.
3. R. Kia, H. Kargar, *J. Coord. Chem.* **2015**, *68*, 1441-1451.
4. M. Ghorbanloo, S. Jafari, R. Bikas, M. S. Krawczyk, T. Lis, *Inorg. Chim. Acta* **2017**, *455*, 15-24.
5. A. D. M. Mohamad, E. R. El-Shrkawy, M. F. I. Al-Hussein, M. S. S. Adam, *J. Taiwan Inst. Chem. Eng.* **2020**, *113*, 27-45.
6. A. H. Kianfar, P. Montazeri Najafabadi, M. Sedighipoor, M. M. Momeni, H. Görls, W. Plass, Gh.

Mohammadnezhad, *Inorg. Chem. Res.* **2021**, *5*, 60-81.
7. J. L. Pratihar, P. Mandal, C. K. Lai, S. Chattopadhyay, *Polyhedron* **2019**, *161*, 317-324.
8. L. L. Li, S. S. Feng, T. Zhang, L. Wang, W. K. Dong, *Inorg. Chim. Acta* **2022**, *534*, 120815.
9. W. N. Ibrahim, M. Shamsuddin, *Crystal Structure Theory and Applications*, **2012**, *1*, 25-29.
10. M. Mirković, M. Radović, D. Stanković, S. Vranješ-Đurić, D. Janković, D. Petrović, L. E. Mihajlović-Lalić, Ž. Prijović, Z. Milanović, *J. Coord. Chem.* **2022**, *75*, 211-224.
11. L. H. Abdel-Rahman, M. S. Adam, N. Al-Zaqri, M. R. Shehata, H. E. Ahmed, S. K. Mohamed, *Arab. J. Chem.* **2022**, *15*, 103737.
12. Z. Shaghaghi, N. Kalantari, M. Kheyrollahpoor, M. Haeili, *J. Mol. Struct.* **2020**, *1200*, 127107.
13. F. Sabate, R. Gavara, I. Giannicchi, R. Bosque, A. D. Cort, L. Rodriguez, *New J. Chem.* **2016**, *40*, 5714-5721.
14. M. S. More, S. B. Pawal, S. R. Lolage, S. S. Chavan, *J. Mol. Struct.* **2017**, *1128*, 419-427.
15. N. Debono, M. Iglesias, F. Sanchez, *Adv. Synth. Catal.* **2007**, *349*, 2470-2476.
16. M. J. Jin, D. H. Lee, *Angew. Chem. Int. Ed.* **2010**, *49*, 1119-1122.
17. C. H. Yang, Y. H. Liu, S. M. Peng, S. T. Liu, *Mol. Catal.* **2022**, *522*, 112232.
18. M. Balali, M. Bagherzadeh, R. Nejat, H. Keypour, *Inorg. Chem. Res.* **2021**, *5*, 82-93.
19. S. R. Borhade, S. B. Waghmode, *Tetrahedron Lett.* **2008**, *49*, 3423-3429.
20. A. M. Tajuddin, H. Bahron, S. N. Ahmad, *Sci. Res. J.* **2015**, *12*, 2-16.
21. S. N. Ahmad, H. Bahron, A. M. Tajuddin, *Int. J. Eng. Technol.* **2018**, *7*, 15-19.
22. R. M. Ansari, B. R. Bhat, *J. Chem. Sci.* **2017**, *129*, 1483-1490.
23. K. E. Balsane, S. S. Shendage, J. M. Nagarkar, *J. Chem. Sci.* **2015**, *127*, 425-431.
24. M. Sedighipoor, A. H. Kianfar, G. Mohammadnezhad, H. Görls, W. Plass, *Inorg. Chim. Acta* **2018**, *476*, 20-26.
25. S. Minakata, M. Komatsu, *Chem. Rev.* **2009**, *109*, 711-724.
26. H. Kargar, M. Moghadam, L. Shariati, N. Feizi, M. Fallah-Mehrjardi, R. Behjatmanesh-Ardakani, K. S. Munawar, *J. Mol. Struct.* **2022**, *1257*, 132608.
27. H. Kargar, A. Moghimi, M. Fallah-Mehrjardi, R. Behjatmanesh-Ardakani, H. Amiri Rudbari, K. S. Munawar, *J. Sulfur Chem.* **2022**, *43*, 22-36.
28. H. Kargar, M. Bazrafshan, M. Fallah-Mehrjardi, R. Behjatmanesh-Ardakani, H. Amiri Rudbari, K. S. Munawar, M. Ashfaq, M. N. Tahir, *Polyhedron* **2021**, *202*, 115194.
29. H. Kargar, P. Forootan, M. Fallah-Mehrjardi, R. Behjatmanesh-Ardakani, H. Amiri Rudbari, K. S. Munawar, M. Ashfaq, M. N. Tahir, *Inorg. Chim. Acta* **2021**, *523*, 120414.
30. H. Kargar, A. Kaka-Naeini, M. Fallah-Mehrjardi, R. Behjatmanesh-Ardakani, H. Amiri Rudbari, K. S. Munawar, *J. Coord. Chem.* **2021**, *74*, 1563-1583.
31. H. Kargar, R. Behjatmanesh-Ardakani, V. Torabi, M. Kashani, Z. Chavoshpour-Natanzi, Z. Kazemi, V. Mirkhani, A. Sahraei, M. N. Tahir, M. Ashfaq, K. S. Munawar, *Polyhedron* **2021**, *195*, 114988.
32. H. Kargar, R. Behjatmanesh-Ardakani, V. Torabi, A. Sarvian, Z. Kazemi, Z. Chavoshpour-Natanzi, V. Mirkhani, A. Sahraei, M. N. Tahir, M. Ashfaq, K. S. Munawar, *Inorg. Chim. Acta* **2021**, *514*, 120004.
33. H. Kargar, V. Torabi, A. Akbari, R. Behjatmanesh-Ardakani, M. N. Tahir, *J. Mol. Struct.* **2019**, *1179*, 732-738.
34. H. Kargar, V. Torabi, A. Akbari, R. Behjatmanesh-Ardakani, M. N. Tahir, *J. Iran. Chem. Soc.* **2019**, *16*, 1081-1090.
35. H. Kargar, V. Torabi, A. Akbari, R. Behjatmanesh-Ardakani, A. Sahraei, M.N. Tahir, *Struct. Chem.* **2019**, *30*, 2289-2299.
36. H. Kargar, M. Fallah-Mehrjardi, *Inorg. Chem. Res.* **2021**, *5*, 201-206.
37. M. Fallah-Mehrjardi, H. Kargar, *Inorg. Chem. Commun.* **2021**, *134*, 109016.
38. Jr. M. J. Frisch, G. W. Trucks, H. B. Schlegel, G. E. Scuseria, M. A. Robb, J. R. Cheeseman, G. Scalmani, etc. GAUSSIAN 09 (Revision D.01) Gaussian, Inc., C. T. Wallingford, **2013**.
39. A. D. Becke, *J. Chem. Phys.* **1993**, *98*, 5648-5652.
40. J. Tomasi, B. Mennucci, R. Cammi, *Chem. Rev.* **2005**, *105*, 2999-3094.
41. F. Weigend, R. Ahlrichs, *Phys. Chem. Chem. Phys.* **2005**, *7*, 3297-3305.
42. J. Gauss, *J. Chem. Phys.* **1993**, *99*, 3629-3643.
43. http://www.chemissian.com.
44. E. D. Glendening, J. K. Badenhoop, A. E. Reed, J. E. Carpenter, J. A. Bohmann, C. M. Morales, C. R. Landis, F. Weinhold, University of Wisconsin, Madison, **2018**.
45. A. Jamshidvand, M. Sahihi, V. Mirkhani, M. Moghadam, I. Mohammadpoor-Baltork, S. Tangestaninejad, H. Amiri Rudbari, H. Kargar, R. Keshavarzi, S. Gharaghani, *J. Mol. Liq.* **2018**, *253*, 61-71.
46. O. A. Blackburn, B. J. Coe, J. Fielden, M. Helliwell, J. J. W. McDouall, M. G. Hutchings, *Inorg. Chem.* **2010**, *49*, 9136-9150.
47. H. Kargar, V. Torabi, A. Akbari, R. Behjatmanesh-Ardakani, A. Sahraei, M. N. Tahir, *J. Mol. Struct.* **2020**, *1205*, 127642.

48. S. Ilhan, H. Temel, I. Yilmaz, M. Sekerci, *Polyhedron* **2007**, *26*, 2795-2802.
49. M. A. Palafox, *Phys. Sci. Rev*. **2018**, *3*, 1-30.
50. C. Tabares-Mendoza, P. Guadarrama, *J. Organomet. Chem.* **2006**, *691*, 2978-2986.
51. P. Geerlings, F. De Proft, W. Langenaeker, *Chem. Rev*. **2003**, *103*, 1793-1874.
52. Z. Demircioğlu, Ç. Albayrak, O. Büyükgüngör, *J. Mol. Struct.* **2014**, *1065-1066*, 210-222.
53. L. Wei, Y. She, Y. Yu, X. Yao, S. Zhang, *J. Mol. Model.* **2012**, *18*, 2483-2491.